ECAP consolidation of Al matrix composites reinforced with in-situ γ-Al_2O_3 nanoparticles

R. Casati [a,*], A. Fabrizi [b], A. Tuissi [c], K. Xia [d], M. Vedani [a]

[a] Department of Mechanical Engineering, Politecnico di Milano, Via La Masa 1, Milano, Italy
[b] Department of Management and Engineering, Università di Padova, Stradella S. Nicola 3, Vicenza, Italy
[c] CNR-IENI, Corso Promessi Sposi 29, Lecco, Italy
[d] Department of Mechanical Engineering, University of Melbourne, Victoria 3010, Australia

Received 2 April 2015
Received in revised form
4 August 2015
Accepted 6 September 2015
Available online 16 September 2015

1. Introduction

Metal matrix nanocomposites (MMnCs) are considered as potential materials for uses in a large number of industrial applications. They provide opportunities to design lightweight structures with tailored balance of mechanical and physical properties, improvement of tribological performance and high temperature strength [1–3]. The reinforcement nanoparticles (NPs) are generally stable at elevated temperatures, making these materials suitable for high temperature applications [4,5]. Thanks to the very small size, the nano-fillers are able to obstruct the movement of dislocations, enabling the Orowan strengthening mechanism [6–8].

Notwithstanding the prospective properties of MMnCs, some aspects of their processing need to be improved. Their fabrication is much more complicated than that of conventional composites reinforced with fibers or micro-sized particles. When the particles scale down from the micro- to the nano-level sizes, new challenges have to be faced. In particular, the high surface energy of NPs readily leads to the formation of clusters which are not effective in hindering the movement of dislocations and result in poor bond with the matrix, thus reducing significantly the strengthening capability of nanoparticles. A number of novel processing routes have been proposed for the synthesis of MMnCs [1–3]. The methods are based either on powder sintering or on liquid processing. Consolidation of particles, generally preceded by high-energy ball milling, can be carried out either by conventional techniques such as hot isostatic pressing and cold isostatic pressing followed by heat treatment or by plastic deformation including equal channel angular pressing (ECAP) and hot extrusion [9–17]. Among the liquid processes, promising results have been achieved by ultrasonic assisted casting [18–20]. Both liquid and solid synthesis methods can be categorized into two classes: the ex-situ and the in-situ synthesis routes. The former refers to those processes in which the nano-reinforcement is added to liquid or powder metal whereas the latter refers to those methods that lead to the formation of nano-sized reinforcement during the process itself, e.g. through reacting gases [1–3].

ECAP is one of the most effective severe plastic deformation techniques, being able to produce metallic materials with ultra-fine grained (UFG) structure. It relies on the introduction of ex-tremely high shear strain during the deformation. Moreover, it has also been used for powder consolidation [21]. Traditional sintering methods are based on diffusion of atoms at the solid state. In contrast, ECAP consolidation mainly relies on very high plastic deformation (especially shear strains) [22]. The high deformation breaks the brittle surface oxide film that covers the particles and leads to direct contact between fresh metal surfaces so that bonding between the particles can occur instantaneously [22]. Fully dense bulk materials are produced thanks to the material

* Corresponding author.
E-mail address: riccardo.casati@polimi.it (R. Casati).

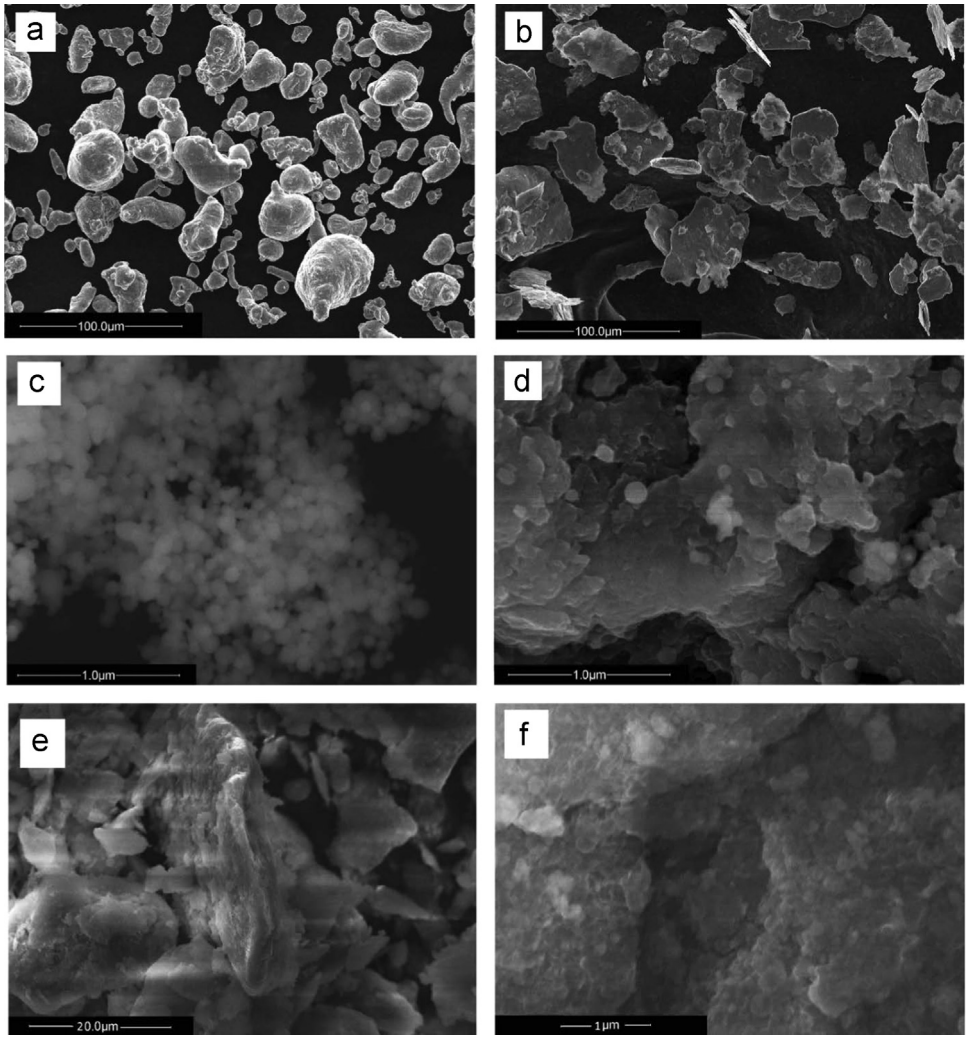

Fig. 1. Micro-sized Al particles in (a) as-received and (b) ball-milled conditions; nano-sized Al particles in (c) as-received and (d) ball-milled conditions; ball-milled mixture of Al micro-particles (50 wt%) and nano-particles (50 wt%) at (e) low and (f) high magnifications.

Table 1
Density values of the consolidated samples.

Consolidated sample	Density (g/cm^3)
As-received Al NPs	2.82
Ball-milled Al NPs	2.80
As-received Al micro-particles	2.70
Ball-milled Al micro-particles	2.70
Ball-milled Al NPs (50 wt%)+Al micro-particles (50 wt%)	2.75

flow accompanying the deformation, which is believed to be able to close the pores between the particles [23]. The application of a back-pressure (BP) is very useful during ECAP consolidation of powdered metals at low temperatures. With the application of a BP, the particles are pushed against each other, generating more friction when passing the shear zone and causing the particles to deform more efficiently instead of just sliding over each other [22]. In this work, Al nano- and micro-particles were employed to prepare, by back-pressure ECAP, Al matrix nanocomposites reinforced with in-situ γ-Al_2O_3 NPs. The pure Al powder was consolidated in the as-received condition and after ball-milling. A milled mixture of Al nano- and micro-powder was also used. The in-situ γ-Al_2O_3 NPs were produced by exploiting the oxide/hydroxide layer that covers the Al particles. The Al nano-sized particles possess higher surface than the micro-sized counterpart.

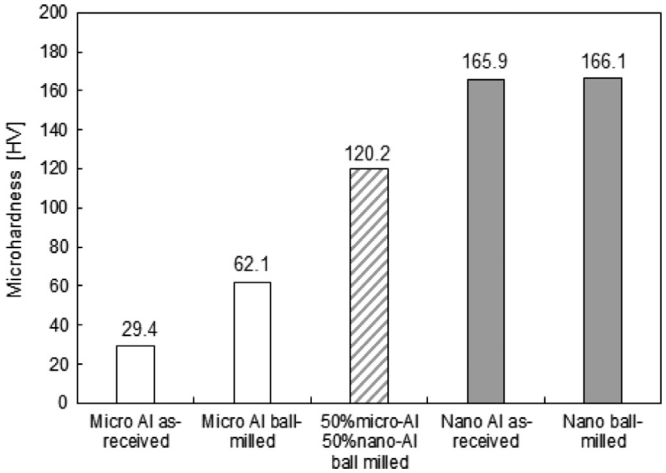

Fig. 2. Vickers microhardness for the ECAP consolidated samples.

This means that they can potentially lead to the production of nanocomposites reinforced with a much higher content of in-situ reinforcement. The morphology of the Al particles, before and after mechanical milling, and the microstructures of the composites were investigated by electron microscopy and X-ray diffraction. The mechanical properties of the final composites were

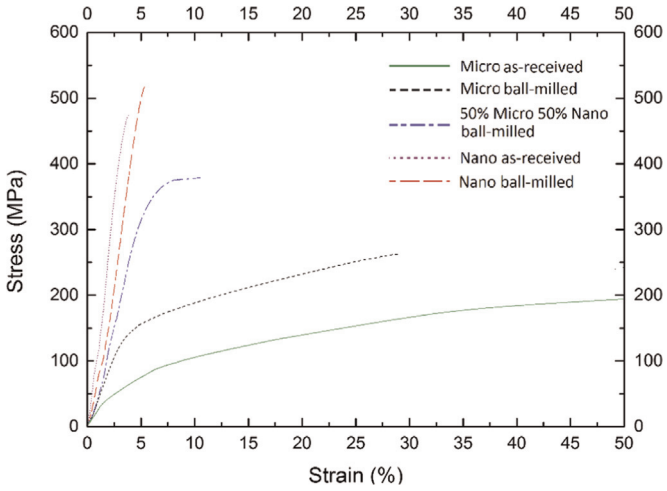

Fig. 3. Compressive stress–strain curves of the ECAP consolidated samples.

evaluated by hardness and compression tests. Particular attention is given to the study of the in-situ phase transformation of the oxide layer into γ-Al_2O_3 NPs, using XRD, differential scanning calorimetry (DSC), and thermo-gravimetric (TG) analysis.

2. Experimental materials and procedures

A commercial purity (CP) micro Al powder with an average size of 20 μm and a nano CP Al powder with an average size of 70 nm were used for the experiments. High-energy ball milling was performed on the Al nano-powder, on the Al micro-powder and on a mixture of 50 wt% of Al nano-powder and 50 wt% of Al micro-powder using a QM-3SP4 planetary mill equipped with stainless steel vials and balls (10 mm in diameter) at 300 rpm. 2 wt% of stearic acid was used as process control agent to avoid excessive cold welding and agglomeration of particles. To minimize oxidation during attrition, the two vials were back-filled with argon. The milling was performed for 16 h with a ball-to-powder weight ratio of 10:1. An excessive temperature rise was avoided by interrupting the procedure for 10 min after each 30 min of milling. After milling, the powders were wrapped in stainless steel foils, cold pressed and subjected to ECAP at 600 °C using a back-pressure of 200 MPa. The pressing speed was 5 mm/min. The ECAP die, with the channels intersecting at 90°, was heated by a resistance heating system and the temperature was controlled using a type-K thermocouple. Four ECAP passes were performed following the C route. The density of the consolidated materials was measured based on the Archimedes' principle using polished samples. Eight measurements were performed for each type of the samples.

Morphological analysis of the powder was performed by a field emission gun scanning electron microscope (FEG-SEM) Philips XL30. The microstructural characterization of the consolidated samples was carried out by transmission electron microscopy (TEM) using a JEM 2000 EX II (JEOL) at 200 kV equipped with energy dispersive spectroscopy (EDS, EDAX) detector. Thin foils, extracted from the transverse section of the ECAP processed billets, were prepared for TEM by grinding and polishing with 6 and 3 μm diamond pastes and colloidal silica suspension. TEM disks (3 mm in diameter, ~25 μm in thickness) were punched from the thin foils and milled by Ar ions using either PIPS 691 or PIPS II (Gatan) devices. Aperture sizes of ~0.8 and 3.5 μm were used to acquire the selected area electron diffraction (SAED) patterns.

X-ray diffraction (XRD) patters were collected using PANalitical X-Pert PRO equipped with a RTMS X'Celerator sensor. Cu Ka (k=0.15418 nm) radiation was employed. Vickers microhardness (HV) was measured using Future Tech Corp. FM-700, applying a 2 N load for 15 s. Compression tests were performed with a crosshead speed of 0.5 mm/min using an MTS Alliance RT/100. The samples were 4 mm in diameter and 6 mm in length. Thermal analyses of powders were performed using a Setaram Labsys TG-DSC-DTA 1600 instrument in a flowing argon atmosphere. Con-tinuous heating experiments were carried out from room tem-perature to 600 °C at a rate of 30 °C/min.

3. Results

3.1. Characterization of powders

The powders were characterized by SEM before and after 16 h ball milling (Fig. 1). In Fig. 1a and c, the as-received micro- and nano-particles are shown. The Al micro-particles appeared rounded and discrete, showing an average size of about 20 μm. The Al NPs were about 80 nm in diameter and almost perfectly spherical. Although they seemed more agglomerated than the micro-particles, the individual NPs were well visible.

The morphologies are consistent with the statement by Ramaswamy [24] that Al particles of 10–20 nm have geometrical shape, while they become spherical as the particle size increases to few tens nanometers. After milling, the particles showed completely different morphologies. The micro-sized particles had a flake morphology (Fig. 1b), while the nanoparticles had aggregated into micro-sized porous clusters although a few discrete spherical nano-particles were still noticeable (Fig. 1d). In Fig. 1e and f, the SEM micrographs of the mixture of the 50% nano- 50% micro-sized particles after ball milling are shown. At a low magnification, they exhibited a flake-like shape while at a high magnification they looked quite similar to the ball-milled nano-sized Al particles.

3.2. Powder consolidation

It was expected that the higher content of surface oxide in the NPs would make their consolidation more difficult. It is also known that in severe plastic deformation, more ductile and bigger particles are easier to shear, thus facilitating the consolidation process while the nano-sized particles are prone to slide over each other instead of being deformed [22]. Processing at high temperatures was therefore required for the consolidation of the nano-Al particles (600 °C). Since a back-pressure helps the ECAP consolidation [22], 200 MPa was applied. After 4 ECAP passes, the particles were fully consolidated and the billets free of cracks. In Table 1, the densities of the consolidated materials are summarized. Higher values are associated with the consolidated Al NP samples because of the higher content of Al oxide (ρ_{aluminum} =2.70 g/cm^3 and ρ_{alumina} =3.96 g/cm^3 [25,26]). How-ever, it is worth noting that the theoretical density of each sample cannot be determined since the actual amount of oxide contained is unknown.

3.3. Mechanical characterization

Vickers microhardness tests were performed on the consolidated samples and summarized in Fig. 2.

The billets consolidated from the nano-sized powder showed remarkably higher hardness (about 166 HV) compared with those samples produced from the micro-sized Al powder. Those prepared from the as-received micro-powder showed a hardness of about 29 HV, while those prepared using the ball-milled micro-powder exhibited a hardness of 62 HV. Finally, the sample produced from a mixture of nano- and micro-particles showed a hardness of about 120 HV, which is the average of the hardness

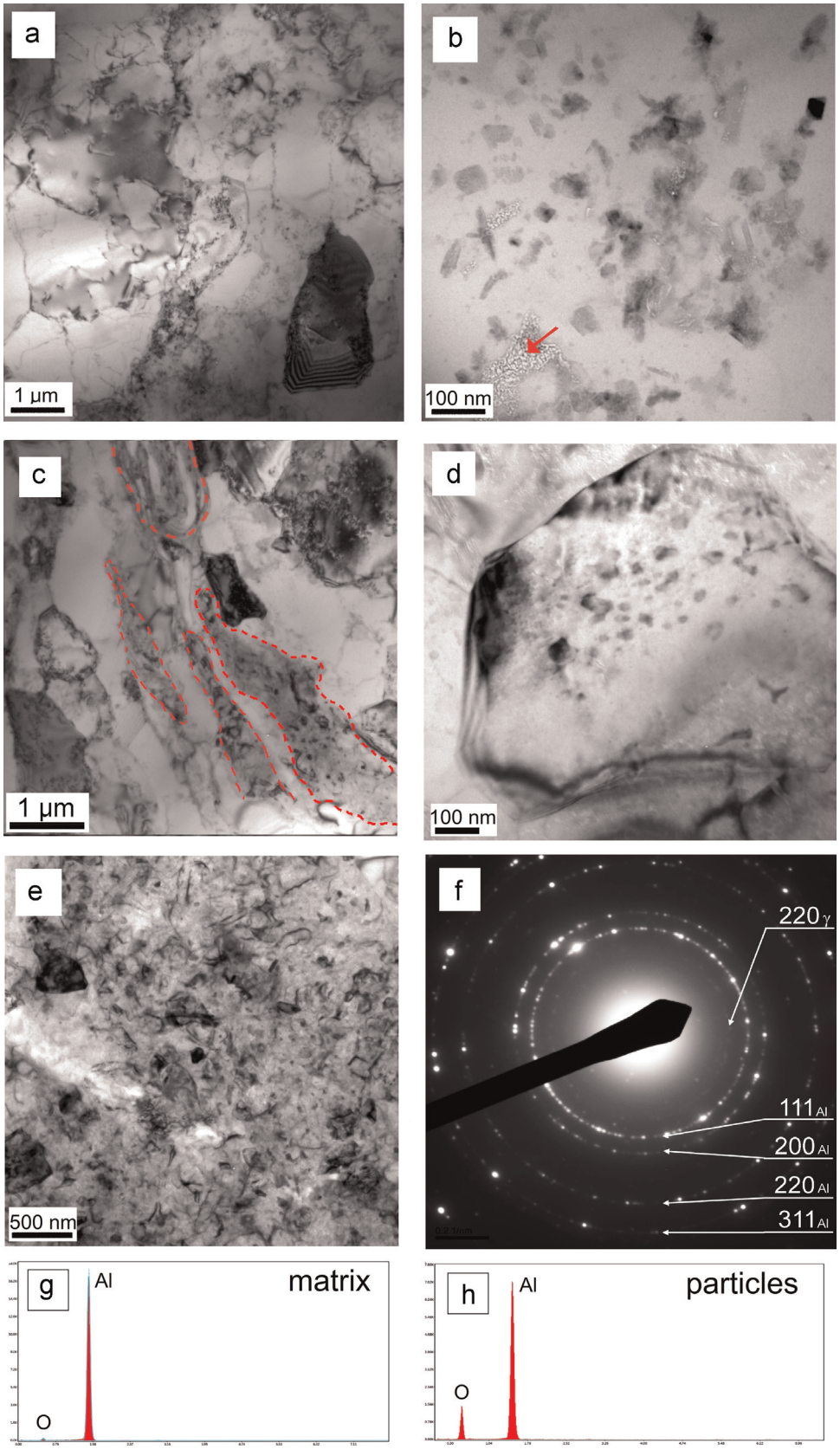

Fig. 4. TEM microstructures of the consolidated samples: (a) and (b) from the as-received micro Al powder; (c)–(e) from the ball milled micro Al powder. (f) SAED pattern identifying the γ-Al_2O_3 NPs and (g) and (h) EDS spectra of the Al matrix and the NPs, respectively, in the sample consolidated from the as-received micro Al powder. (For interpretation of the references to color in the text, the reader is referred to the web version of this article.)

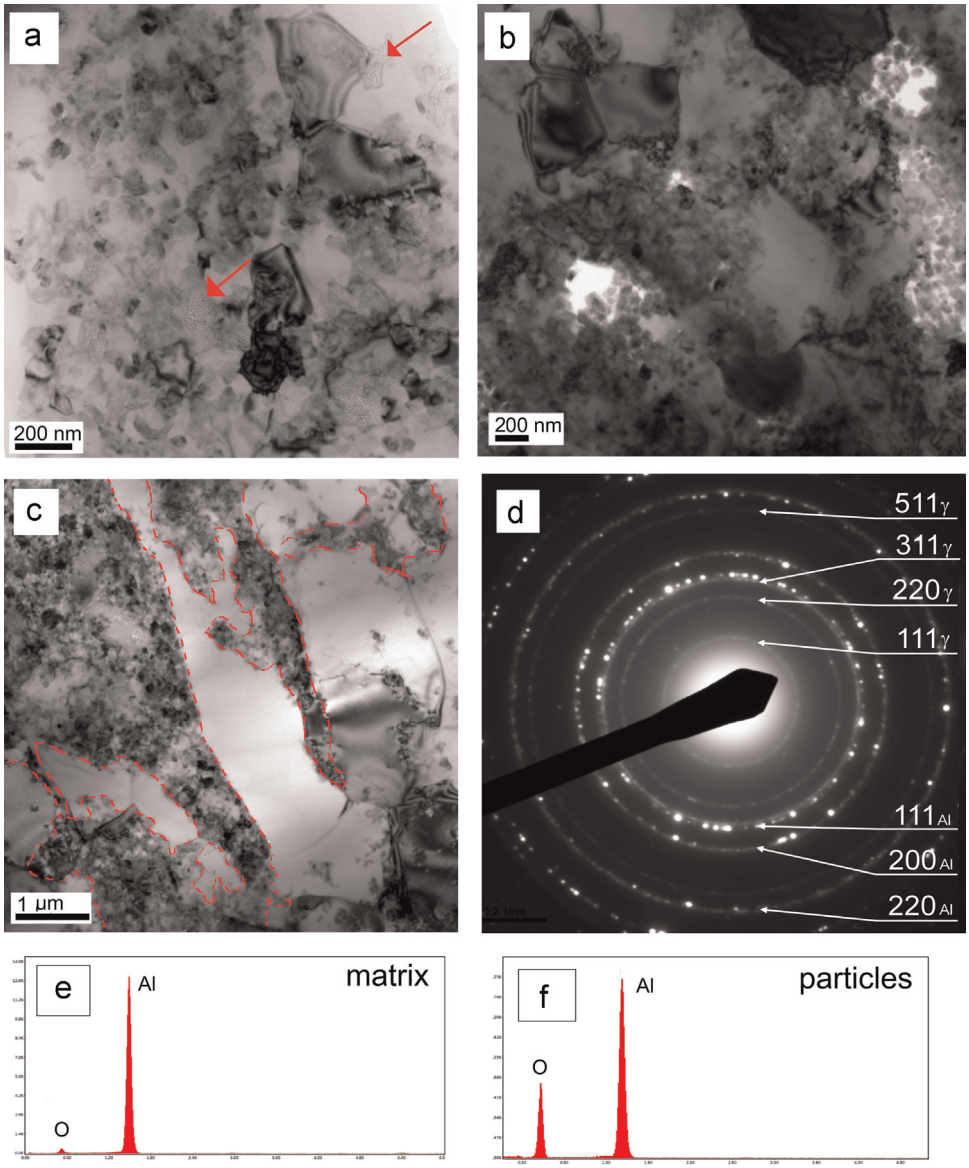

Fig. 5. Microstructures of the consolidated samples: (a) from the as-received nano Al powder, (b) from the ball milled nano Al powder, and (c) from the ball-milled mixture of micro and nano Al powders. (d) SAED pattern identifying γ-Al_2O_3 and (e) and (f) EDS spectra of the Al matrix and the NPs. (For interpretation of the references to color in the text, the reader is referred to the web version of this article.)

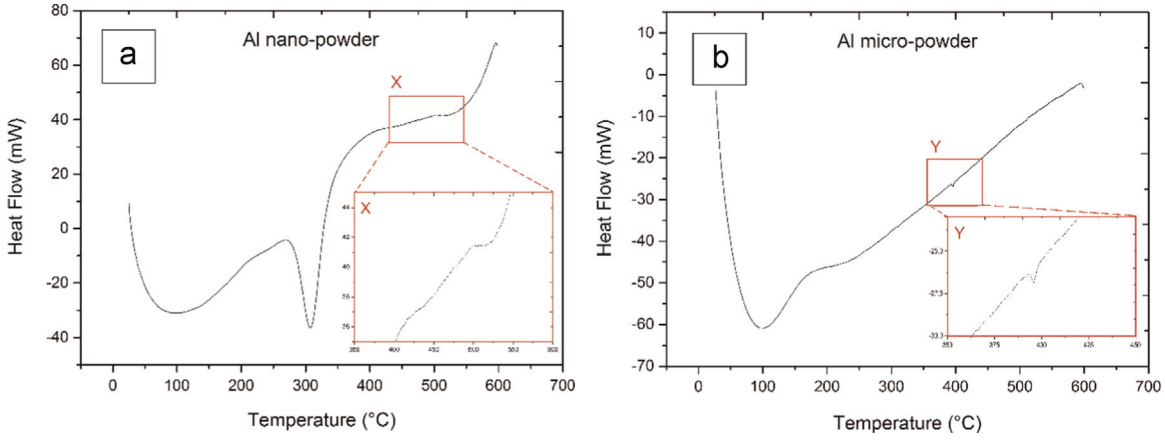

Fig. 6. (a) DSC curve for the nano Al powder with the inset showing a magnified section in area X. (b) DSC curve for the micro Al powder with the inset showing a magnified section in area Y.

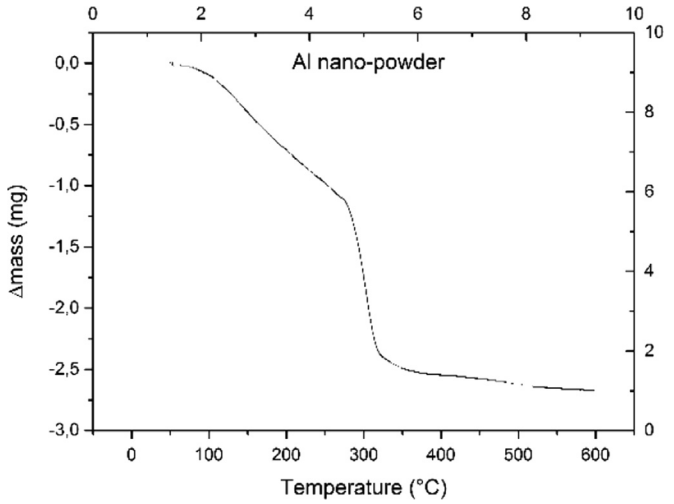

Fig. 7. TG curve for the nano Al powder.

values of the other two ball milled samples.

In Fig. 3, the compressive stress–strain curves are displayed. The samples originated from the nano-sized powders showed a brittle behavior but an extremely high strength. Indeed, they broke before reaching the macroscopic yielding point. The samples originated from the micro-sized powders showed a ductile behavior but much lower strengths. The consolidated ball-milled micro-Al powder reached a compressive yield stress of about 140 MPa and an elongation of 28%. The consolidated as-received micro-Al powder reached a compressive yield stress of about 40 MPa and the test was stopped at 50% of strain without fracture. Again, the sample from the mixed powder displayed ductility and strength in between, with compressive yield stress and ductility of about 350 MPa and 11%, respectively.

3.4. Microstructural characterization of ECAP consolidated samples and powder

A typical TEM microstructure of the sample consolidated from the as-received micro Al powder is depicted in Fig. 4a. Quasi-equiaxed grains with homogeneous sizes (about 3 μm) are observed in the whole investigated area. Discrete NPs and small clusters are found dispersed within the grains and at the grain boundaries, as shown in Fig. 4a and b. EDS analysis revealed that the NPs are oxygen-rich compounds (Fig. 4g and h). The NPs were identified as γ-Al_2O_3 by the SAED pattern (Fig. 4f). The original oxygen-rich surfaces of the starting particles were not noticeable although they were observed in the samples consolidated at lower temperatures as shown in some previous works [27–29]. Therefore, the observed NPs are expected to be oxide compounds originating from the amorphous oxide layer [30–37] that covers the Al particles. This aspect will be further investigated and discussed.

The microstructures of the consolidated sample from the ball-milled micro Al powder are shown in Fig. 4(c–e), showing coarse grains with average size between 1 and 3 μm (Fig. 4c) and some finer structures (indicated in Fig. 4c by the red dashed lines). The latter is characterized by a high-density of oxide NPs, submicron Al grains and a high amount of microstructural defects (Fig. 4e). Some micro-sized grains, especially those between two zones with high contents of oxide particles, show elongated shape. It is worth noting that NPs are present not only in the areas with finer structures, but also dispersed in some coarser grains, as displayed in Fig. 4d. The NPs are again identified as γ-Al_2O_3.

In Fig. 5a and b, the microstructures of the consolidated samples produced from the as-received and ball-milled nano Al powders are depicted, respectively. The two microstructures look quite similar and the effect of the ball milling was not as marked as in the case of the micro-sized Al powder. In some areas, small grains (lower than 1 μm in size) are detected. In some other areas, grain boundaries are not easily identified because of the high density of oxide NPs which are again indexed as γ-Al_2O_3 (Fig. 5d–f).

The billet consolidated from the ball milled mixture of the micro and nano powders showed a bimodal microstructure (Fig. 5c). The micro-sized grains are separated by zones of nano-sized grains and high amount of oxide NPs (indicated by the red dashed lines in Fig. 5c).

Finally, it is worth noting that in all the materials, a small number of oxygen-rich amorphous NPs are detected, as indicated by the red arrows in Figs. 4b and 5a. Several reports show that the Al particles are covered by an amorphous oxide layer 2–4 nm thick [27,30–37], therefore a phase transformation from an amorphous- to a γ- phase occurred during the consolidation process. TG, DSC and more XRD were performed to shed further light on the formation of γ-Al_2O_3 NPs.

In Fig. 6a, the DSC curve for the as-received nano Al powder shows an intense endothermic peak between 275 and 370 °C and a weak exothermic peak between 470 and 530 °C. In contrast, in Fig. 6b, the DSC curve for the as-received micro Al powder shows just a weak endothermic peak between 391 and 399 °C.

The TG measurement performed on the nano Al powder showed a reduction of mass in the first stage of heating (100 to 300 °C), a drastic loss of mass at ~300 °C corresponding to the DSC endothermic peak and then a region featuring a mass loss at a much slower rate (Fig. 7).

XRD was carried out at 25, 200 (below the DSC endothermic peak), 400 (between the DSC endothermic and exothermic peaks) and 600 °C (the ECAP temperature which is above the DSC exothermic peak) to acquire information about phase stability. As mentioned, 600 °C is the ECAP processing temperature.

Fig. 8a and b display the patterns for the as-received nano Al powder at 25 and 200 °C. The peaks of Al and aluminum trihydroxide γ-$Al(OH)_3$ were identified. The γ-$Al(OH)_3$ phase is also known as gibbsite and possesses a monoclinic symmetry with the space group P21/n. At 400 °C, the peaks of the hydroxide dis-appeared and only those of Al were detected (Fig. 8c). Finally, at 600 °C the loose nano Al powder showed both the peaks of Al and γ-Al_2O_3 phases (Fig. 8d). By zooming the XRD pattern at 400 °C, an hump related to an amorphous phase is visible at low incident angles, where the peaks of the $Al(OH)_3$ and γ-Al_2O_3 are present at 25 °C and 600 °C, respectively (see for comparison Fig. 8e and f). XRD was also performed on the micro Al powder, but the only Al peaks were detected (Fig. 9). A shift of the angular peak positions toward lower angles was noticeable with increasing temperature, most probably due to a thermal drift. The specific surface of the micro Al particles is much lower than that of the nano Al particles; therefore, the amount of oxide/hydroxide growing on their surface is believed to be not enough to be detected.

4. Discussion

Aluminum is thermodynamically unstable with respect to its oxide and hydroxide in air. Both bulk Al and particles are naturally covered by an amorphous oxide layer which is about 2–4 nm thick at room temperature [27,30–37]. This layer is very compact and stable and protects the interior from further oxidation. Growth of the amorphous oxide layer is limited by the outward diffusion of Al cations [38]. The amorphous alumina layer becomes metastable when the thickness exceeds a threshold value [39,40]. Besides, it is largely accepted that the chemical reactivity of aluminum and

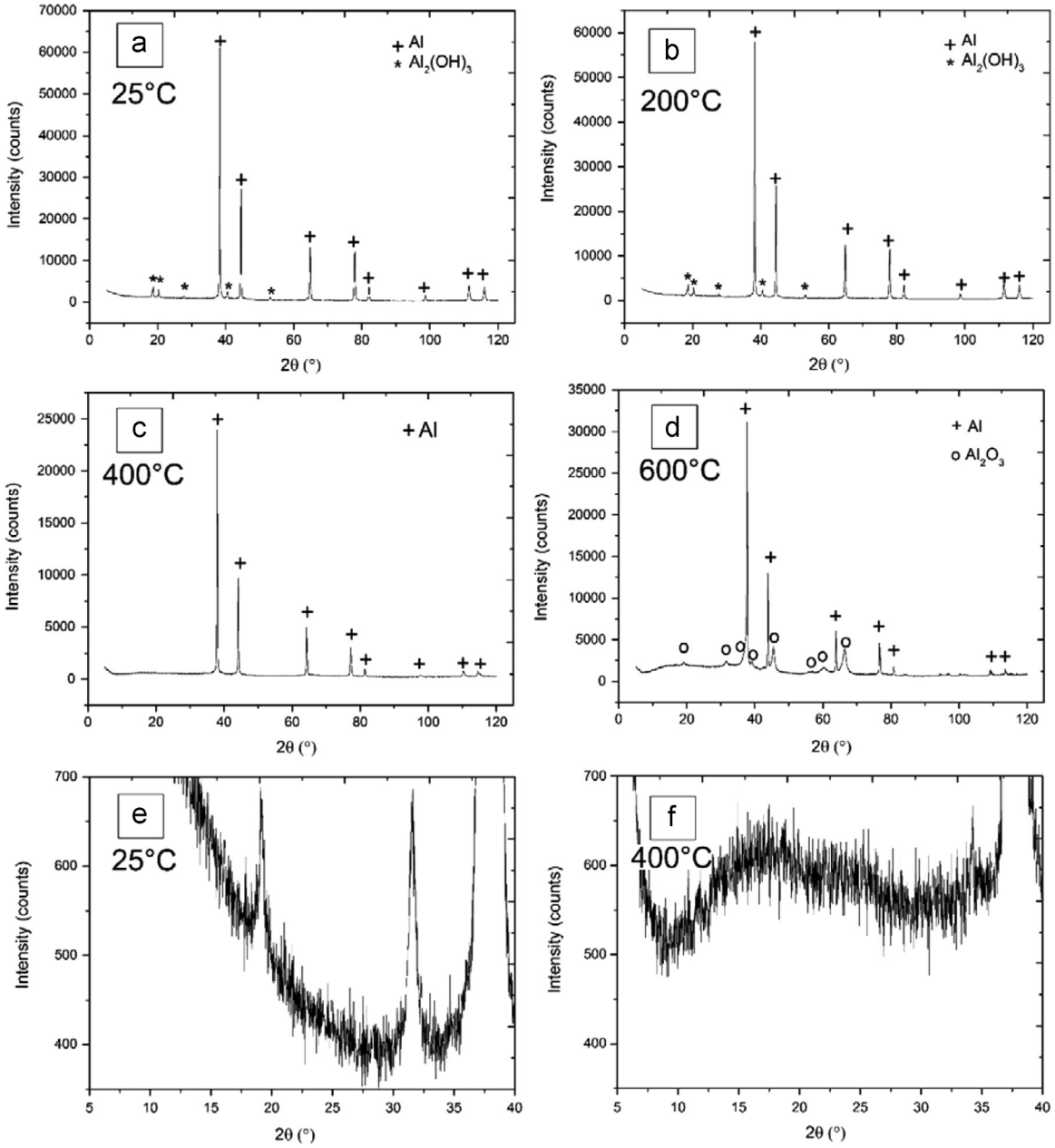

Fig. 8. XRD patterns for the as-received nano Al powder: (a) at 25 °C, (b) at 200 °C, (c) at 400 °C, and (d) at 600 °C. Closeups between 5° and 40° are shown (e) at 25 °C and (f) at 400 °C.

other metals at the nanometer scale differs from that measurable at the macroscopic level; indeed different transformations and reactions may happen at the nano-scale, which are not favored at the micro-scale [41–45]. The small size and large surface area provide a significantly high chemical reactivity. For example, passive bulk aluminum is practically stable, even in boiling water [33], but nano-sized Al particles react with water to form aluminum hydroxide, releasing H_2 [46]. There is also some evidence that Al trihydroxide can form during prolonged exposure to humid environment in the outermost passive layer of bulk Al samples [47–49]. This reaction is likely to happen more decisively on the Al nanoparticles. Moreover, the oxide on the Al nanoparticles is revealed to be more porous than that on the micro-sized Al particles and potentially able to absorb larger amounts of atmospheric moisture [24]. In agreement with these observations, XRD revealed that an aluminum hydroxide layer (gibbsite) covers the Al nanoparticles used in the present experiments.

When the Al NPs are heated, they undergo an endothermic transformation between 275 and 370 °C. At 200 °C, the peaks of gibbsite were still very much visible, whereas at 400 °C they disappeared. The endothermic transformation is attributed to the dehydration of the trihydroxide, causing its transformation into alumina and water according to

$$2Al(OH)_3 \rightarrow Al_2O_3 + 3H_2O \quad (1)$$

The DSC results are in good agreement with some previous works on dehydration of gibbsite [50–53]. The occurrence of dehydration is also supported by the TG results (Fig. 7), which show a drastic reduction of weight corresponding to the endothermic peak, confirming the loss of H_2O molecules during the dehydration reaction. Furthermore, the loss in weight visible in the first part of the curve can be ascribed to the evaporation of the adsorbed water. XRD carried out at 400 °C on nano Al particles exhibited

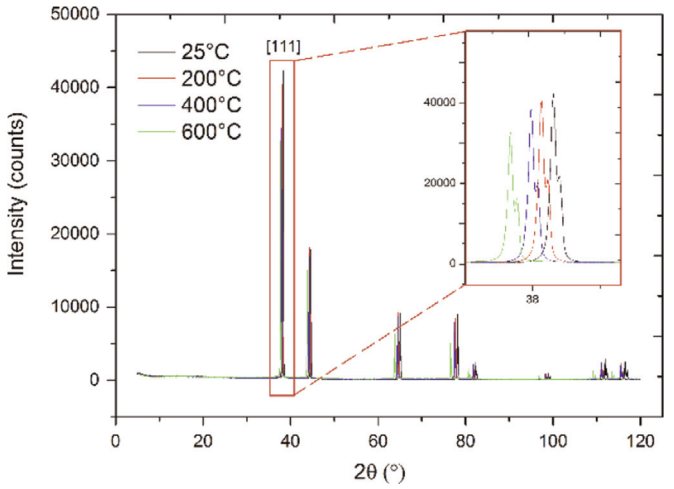

Fig. 9. XRD pattern for the as-received micro Al powder at 25, 200, 400 and 600 °C. A closeup in correspondence of the [111] peak is depicted in the inset.

only the peaks of the face-centered cubic Al structure. No characteristic peaks for crystalline-Al_2O_3 were noticeable, and a broad hump ascribable to an amorphous phase was visible at low incident angles (see for comparison Fig. 8e and f).

Dehydration is a very complex process, which leads to the loss of the long-range order in the crystal structure [54]. The transformations gibbsite→amorphous Al_2O_3 and gibbsite→boehmite (γ-AlOOH)→amorphous Al_2O_3 were proposed for gibbsite particles [33,52,54–56]. The formation of the amorphous Al_2O_3 is an intermediate stage between the solid-state reaction from gibbsite to the crystalline alumina. The gibbsite structure is distorted during its dehydration/amorphization, causing the variation and loss of the cell parameters and the loss of the long-range crystal order due to structural reordering and the loss of water [53,54]. At 600 °C, the peaks of γ-Al_2O_3 were detected in the powder and consolidated samples. Therefore, between 400 and 600 °C the amorphous phase transforms into a crystalline structure. As shown in Fig. 5a, a small exothermic peak between 470 °C and 530 °C was detected by DSC analysis on the nano-Al particles. This peak might be assigned to the amorphous Al_2O_3→γ-Al_2O_3 transformation. However, it is worth noting that some other phenomena could cause exothermic heat release, namely residual oxidation, annealing of defects or strain relaxation in the Al particle core. Accelerated oxidation was observed by Trunov et al. [57] in a narrow range from 550 and 650 °C below the Al melting temperature, when a critical value of the oxide thickness (4 nm) is exceeded. It is suggested that the newly formed γ-Al_2O_3 has a density 20% higher than that of the amorphous-Al_2O_3. Thus, the cubic alumina does not fully cover the Al particle surface. The formation of bare Al spots and their immediate oxidation may cause the rapid increase of oxide until a continuous layer is formed. It is estimated that the thickness of the γ-Al_2O_3 layer is about 15–20 nm. It is noted that on the TG curve in Fig. 7, the increase in mass is not evident because the test was carried out in Ar atmosphere. Thus, at 600 °C, the content of Al oxide is expected to be higher than that in the as-received powder and the amount of oxide in the consolidated sample has to be even higher.

The diffraction peaks of Al_2O_3 and $Al(OH)_3$ were detected only for the nano Al powder. The amount of these phases is believed to be too low to detect in the micro Al powder. A weak endothermic DSC peak was noticeable between 391 and 399 °C when the mi-cro-sized powder underwent the heating scan (Fig. 6b). This might suggest the presence of some hydroxide on the surface that transformed into amorphous Al_2O_3, but there is no XRD evidence. Nonetheless, according to the results achieved using the nano Al particles, no matter whether the Al particles were covered by the hydroxide at low temperatures (< 400 °C), at the consolidation temperature of 600 °C, a γ-Al_2O_3 layer is supposed to cover the metal particles.

In Figs. 4 and 5, it was shown that the oxide phase was not present as boundaries between the original Al particles, as

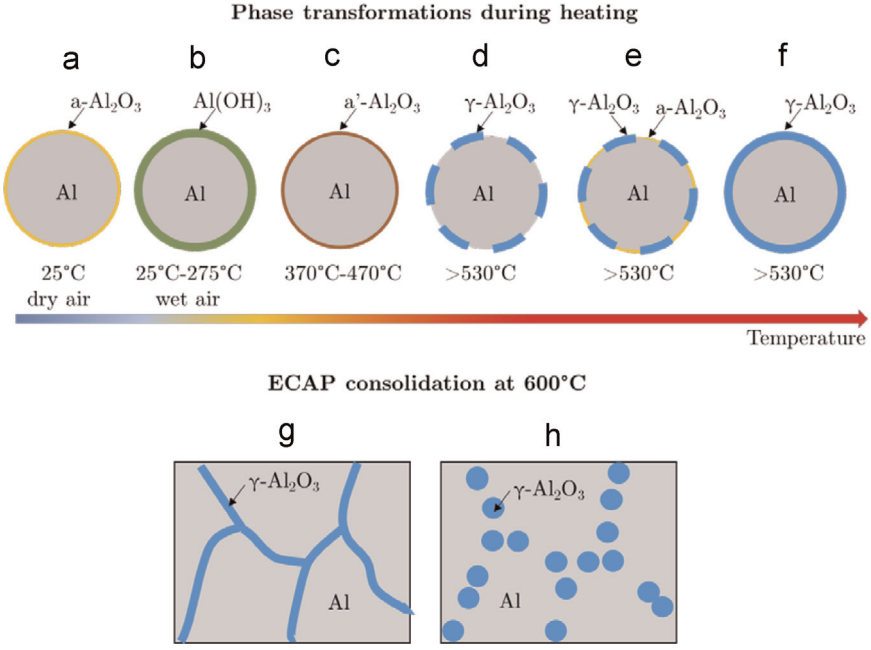

Fig. 10. Schematic of the transformation of the oxide layer: (a) a nano Al particle is covered by an amorphous oxide layer 2–4 nm thick at room temperature (a-Al_2O_3), (b) as soon as they are exposed to atmospheric moisture the oxide reacts with water to form aluminum hydroxide ($Al(OH)_3$, (c) between 275 and 370 °C, the hydroxide dehydrates and loose its long range crystallographic order, forming amorphous alumina (a′- Al_2O_3) which remains stable below 470 °C, (d) between 470 and 530 °C, a′-Al_2O_3 transforms into γ-Al_2O_3 which has a density 20% higher than that of a-Al_2O_3, leading to its not fully covering the Al particle surface, (e,f) the bare Al spots and their immediate oxidation may cause the rapid increase of oxide until a continuous layer is formed, and (g,h) when the nano Al particles are consolidated by ECAP at 600 °C, the continuous γ-Al_2O_3 layers transform into discrete γ-Al_2O_3 NPs to minimize the surface energy. The ECAP process plays a role in dispersing the NPs.

previously found in samples consolidated at 400 °C [27] or even lower temperatures [28,29]. The oxide was found, indeed, in the form of particles well dispersed in the metal matrix in all the samples investigated. γ-Al_2O_3 NPs were also obtained by Balog et al. after annealing of the consolidated micro Al powder (1–9 μm) at temperatures higher than 450 °C [27]. The driving force for the transformation from oxide layers into oxide particles is considered to be the minimization of surface energy, which is made possible by diffusion at the higher temperatures. The ECAP process also play a role in dispersing the NPs [22]. The transformation process from the oxide layer into discrete γ-Al_2O_3 NPs can be summarize in eight steps, as illustrated in Fig. 10.

The microstructures observed in the present study correspond well with the mechanical properties obtained. The very high content of reinforcing γ-Al_2O_3 NPs in the materials produced from nano Al particles plausibly leads to their extraordinary high hardness (about 166 HV), low ductility and high compressive strength (Figs. 2 and 3). For comparison, it is worth reporting that the Vickers hardness of coarse-grained and UFG pure aluminum are about 20 HV and 40 HV, respectively [58]. The in-situ reinforcement led to a hardness increase of about 400% when compared with the unreinforced UFG Al.

The samples produced from the micro Al powder, reinforced with lower amounts of alumina NPs, showed much lower hardness and strength but higher ductility. The samples prepared from the as-received powder showed a hardness of about 29 HV and a yield strength of 40 MPa while those prepared using the ball-milled powder exhibited a hardness of 62 HV and a yield stress of 140 MPa. The hardness values are consistent with previous results achieved by consolidating Al particles at lower temperature [59]. The as-received and ball-milled Al powder consolidated by ECAP for 4 passes at 400 °C showed higher Vickers hardness (37 HV and 93 HV, respectively [59]) due to a softer annealing action exerted during holding at the processing temperature. Finally, the sample produced from the mixture of nano- and micro-particles showed a hardness of about 120 HV, a yield stress of about 350 MPa and a ductility of 11%, representing a compromise between those achieved by the samples produced using the ball-milled micro-sized Al powder and the ball-milled nano-sized Al powder. This might suggest the possibility of using different proportions of nano- and micro-particles in order to produce the desired combinations of mechanical properties.

The enhanced hardness and strength are due to the strengthening effect of the dispersed nanoparticles and of the refined microstructure [6–8,21]. The nanoparticles can interact with dislocations, hampering their movement and leading to dislocations bowing around the particles (Orowan strengthening) [6–7]. The mismatch in the coefficient of thermal expansion between the reinforcement and the metal matrix is also believed to contribute to strengthening since it leads to the formation of dislocations, which are geometrically necessary to accommodate the different contractions [8,60]. Moreover, the grain size has a strong influence on strength since the grain boundaries can obstruct dislocation movement [21], and the particles play an important role in refining grains in the composites because they can hinder grain growth at high temperatures by acting as pinning points for grain boundary migration. The effect of the finer grain size is demonstrated in the sample produced from ball milled micro Al powder, which showed higher strength and hardness than that produced from as-received powder.

5. Conclusions

A method to prepare MMnCs reinforced with in-situ γ-Al_2O_3 NPs was applied. Five different composites were produced using micro- and nano-sized Al powders either in the as-received conditions or after high-energy ball milling. The consolidation process was carried out at 600 °C by ECAP with a back pressure of 200 MPa. The reinforcing NPs were produced in-situ from the surface oxide layer via the following transformation path: a-$Al_2O_3 \rightarrow Al(OH)_3 \rightarrow a'$-$Al_2O_3 \rightarrow \gamma$-$Al_2O_3$. The Al nanoparticles are covered by an amorphous oxide layer 2–4 nm thick at room temperature (a-Al_2O_3) which reacts with water to form aluminum hydroxide ($Al(OH)_3$) as soon as it is exposed to atmospheric moisture. Between 275 and 370 °C, the hydroxide dehydrates and loose its long range crystallographic order, forming amorphous alumina (a′-Al2O3). Between 470 and 530 °C, the amorphous-Al_2O_3 transforms into γ-Al_2O_3 with increasing thickness. During ECAP consolidation at 600 °C, the continuous γ-Al_2O_3 layers transform into discrete γ-Al_2O_3 NPs to minimize the surface energy. The ECAP process also plays a role in dispersing the NPs.

The composites consolidated from the nano-sized powder showed remarkably higher hardness (about 166 HV) than those prepared from the micro-sized Al powder (29 HV). The samples produced using nano-sized powder showed a brittle behavior but an extremely high strength in compression while those produced using the micro-sized powders showed a ductile behavior but much lower strength. The sample consolidated from the ball-milled mixture of the micro and nano Al particles displayed a very interesting mechanical behavior that is a compromise between ductility and strength (11% and 350 MPa, respectively). The enhanced hardness and strength are believe to be due to the strengthening effect of the dispersed nanoparticles and of the refined microstructure.

References

[1] S.C. Tjong, Novel nanoparticle-reinforced metal matrix composites with enhanced mechanical properties, Adv. Eng. Mater. 9 (2007) 639–652.
[2] S.R. Bakshi, D. Lahiri, A. Agarwal, Carbon nanotube reinforced metal composites – a review, Int. Mater. Rev. 55 (2010) 42–64.
[3] R. Casati, M. Vedani, Metal matrix composites reinforced by nano-particles – a review, Metals 4 (1) (2014) 65–83.
[4] S.H. Wang, P.W. Kao, The strengthening effect of Al_3Ti in high temperature deformation of Al–Al_3Ti composites, Acta Mater. 46 (1998) 2675–2682.
[5] R.A. Varin, Intermetallic-reinforced light-metal matrix in-situ composites, Metall. Mater. Trans. A: Phys. Metall. Mater. Sci. 33 (2002) 193–201.
[6] Z. Zhang, D.L. Chen, Contribution of Orowan strengthening effect in particulate-reinforced metal matrix nanocomposites, Mater. Sci. Eng.: A 483–484 (2008) 148–152.
[7] Z.Y. Ma, Y.L. Li, Y. Liang, F. Zheng, J. Bi, S.C. Tjong, Nanometric Si_3N_4 particulate-reinforced aluminum composite, Mater. Sci. Eng.: A 219 (1996) 229–231.
[8] R. Casati, M. Amadio, C.A. Biffi, M. Vedani, D. Dellasega, A. Tuissi, Al/Al_2O_3 nanocomposite produced by ECAP, Mater. Sci. Forum 762 (2013) 457–464.
[9] C. Carreño-Gallardo, I. Estrada-Guel, M. Romero-Romo, R. Cruz-García, C. López-Meléndez, R. Martínez-Sánchez, Characterization of Al_2O_3NP–Al2024 and AgCNP–Al2024 composites prepared by mechanical processing in a high energy ball mill, J. Alloy. Compd. 536 (2012) S26–S30.
[10] L. Kollo, M. Leparoux, C.R. Bradbury, C. Jäggi, E. Carreño-Morelli, M. Rodríguez-Arbaizar, Investigation of planetary milling for nano-silicon carbide reinforced aluminium metal matrix composites, J. Alloy. Compd. 489 (2010) 394–400.
[11] M.O. Lai, L. Lu, W. Laing, Formation of magnesium nanocomposite via mechanical milling, Compos. Struct. 66 (2004) 301–304.
[12] D. Bozic, J. Stasic, B. Dimcic, M. Vilotijevic, V. Rajkovic, Multiple strengthening mechanisms in nanoparticle-reinforced copper matrix composites, J. Mater. Sci. 34 (2011) 217–226.
[13] F. Zhang, W.A. Kacmarek, L. Lu, M.O. Lai, Formation of Al TiN metal matrix composite via mechanochemical route, Scr. Mater. 43 (2000) 1097–1102.
[14] R. Casati, X. Wei, K. Xia, D. Dellasega, A. Tuissi, E. Villa, M. Vedani, Mechanical and functional properties of ultrafine grained Al wires reinforced by nano-Al_2O_3, Mater. Des. 64 (2014) 102–109.
[15] P. Quang, Y.G. Jeong, S.C. Yoon, S.H. Hong, H.S. Kim, Consolidation of 1 vol% carbon nanotube reinforced metal matrix nanocomposites via equal channel angular pressing, J. Mater. Process. Technol. 187–188 (2007) 318–320.
[16] M. Mozaffari, M. Gheisari, M. Niyaifar, J. Amighian, Magnetic properties of mechanochemically prepared iron–wustite (Fe–FeyO) nanocomposites, J. Magn. Magn. Mater. 321 (2009) 2981–2984.
[17] M. Balog, F. Simancik, O. Bajana, G. Requena, ECAP vs. direct extrusion—techniques for consolidation of ultra-fine Al particles, Mater. Sci. Eng.: A 504

(2014) 1–7.
[18] X. Li, Y. Yang, X. Cheng, Ultrasonic-assisted fabrication of metal matrix composites, J. Mater. Sci. 39 (2004) 3211–3212.
[19] M. De Cicco, L. Turng, X. Li, J.H. Perepezko, Nucleation catalysis in aluminum alloy A356 using nanoscale inoculants, Metall. Mater. Trans. A 42 (2011) 2323–2330.
[20] M. De Cicco, L. Turng, X. Li, J.H. Perepezko, Production of semi-solid slurry through heterogeneous nucleation in metal matrix nanocomposites (MMNC) using nano-scaled ultrasonically dispersed inoculants, Solid State Phenom. 141–143 (2008) 487–492.
[21] S. Xiang, K. Matsuki, N. Takatsuji, M. Tokizawa, T. Yokote, J. Kusui, K. Yokoe, Microstructure and mechanical properties of pm 2024Al–3Fe–5Ni alloy consolidated by a new process, equal channel angular pressing, J. Mater. Sci. Lett. 16 (1997) 1725–1727.
[22] X. Xia, Consolidation of particles by severe plastic deformation: mechanism and applications in processing bulk ultrafine and nanostructured alloys and composites, Adv. Eng. Mater. 12 (2010) 724–729.
[23] R. Lapovok, D. Tomus, C. Bettles, Shear deformation with imposed hydrostatic pressure for enhanced compaction of powder, Scr. Mater. 58 (2008) 898–901.
[24] A.L. Ramaswamy, P. Kaste, S.F. Trevino, A "micro-vision" of the physio-chemical phenomena occurring in nanoparticles of aluminum, J. Energ. Mater. 21 (2004) 1–24.
[25] ASM handbook, vol. 2.
[26] ASM handbook, vol. 21.
[27] M. Balog, P. Krizik, M. Nosko, Z. Hajovska, M.V. Castro Riglo, W. Rajnerc, D.-S.-Liu, F. Simancik Forged, HITEMAL: Al-based MMCs strengthened with nanometric thick Al_2O_3 skeleton, Mater. Sci. Eng. A 613 (2014) 82–90.
[28] X. Wu, W. Xu, K. Xia, Pure aluminum with different grain size distributions by consolidation of particles using equal-channel angular pressing with back pressure, Mater. Sci. Eng. A 493 (2008) 241–245.
[29] W. Xu, X. Wu, T. Honma, S.P. Ringer, K. Xia, Nanostructured Al–Al_2O_3 composite formed in situ during consolidation of ultrafine Al particles by back pressure equal channel angular pressing, Acta Mater. 57 (2009) 4321–4330.
[30] M.A. Trunoc, M. Schoenitz, X. Zhu, E.L. Dreizin, Effect of polymorphic phase transformations in Al_2O_3 film on oxidation kinetics of aluminum powders, Combust. Flame 140 (2005) 310–318.
[31] X. Phung, J. Groza, E.A. Stach, L.N. Williams, S.B. Ritchey, Surface characterization of metal nanoparticles, Mater. Sci. Eng.: A 359 (2003) 261–268.
[32] M. Balog, F. Simancik, M. Walcher, W. Rajner, C. Poletti, Extruded Al–Al_2O_3 composites formed in situ during consolidation of ultrafine Al powders: effect of the powder surface area, Mater. Sci. Eng.: A 529 (2011) 131–137.
[33] K. Wafers, C. Misra, Oxides and Hydroxides of Aluminum, Alcoa Technical Report No. 19 Revised, Alcoa Laboratories, 64, 1987.
[34] B. Rufino, F. Boulc'h, M.V. Coulet, G. Lacroix, R. Denoyel, Influence of particles size on thermal properties of aluminium powder, Acta Mater. 55 (2007) 2815–2827.
[35] J.C. Sanchez-Lopez, A.R. Gonzalez-Elipe, A. Fernandez, Passivation of nanocrystalline Al prepared by the gas phase condensation method: an x-ray photoelectron spectroscopy study, J. Mater. Res. 13 (1998) 703–710.
[36] P.E. Doherty, R.S. Davis, Direct observation of the oxidation of aluminum single-crystal surfaces, J. Appl. Phys. 34 (1963) 619–628.
[37] K. Tomas, M.W. Roberts, Direct observation in the electron microscope of oxide layers on aluminum, J. Appl. Phys. 32 (1961) 70–75.
[38] L.P.H. Jeurgens, W.G. Sloof, F.D. Tichelaar, E.J. Mittemeijer, Growth kinetics and mechanisms of aluminum-oxide films formed by thermal oxidation of aluminum, J. Appl. Phys. 92 (2002) 1649–1656.
[39] L.P.H. Jeurgens, W.G. Sloof, F.D. Tichelaar, E.J. Mittemeijer, Thermodynamic stability of amorphous oxide films on metals: application to aluminum oxide films on aluminum substrates, Phys. Rev.: B 62 (2000) 4707–4719.
[40] B. Rufino, F. Boulc'h, M.V. Coulet, G. Lacroix, R. Denoyel, Influence of particles size on thermal properties of aluminum powder, Acta Mater. 55 (2007) 2815–2827.
[41] L. Meda, G. Marra, L. Galfetti, F. Severini, L. De Luca, Nano-aluminum as energetic material for rocket propellants, Mater. Sci. Eng.: C 27 (2007) 1393–1396.
[42] B.J. Henz, T. Hawa, M.R. Zachariah, On the role of built-in electric fields on the ignition of oxide coated nanoaluminum ion mobility versus Fickian diffusion, J. Appl. Phys. 107 (2010) 024901.
[43] M. Valden, X. Lai, D.W. Goodman, Onset of catalytic activity of gold clusters on titania with the appearance of nonmetallic properties, Science 281 (1998) 1647–1650.
[44] Y. Yang, S. Wang, Z. Sun, D.D. Dlott, Near-infrared laser ablation of poly tetrafluoroethylene (teflon) sensitized by nanoenergetic materials, Appl. Phys. Lett. 85 (2004) 1493–1495.
[45] B. Yoon, H. Hakkinen, U. Landman, A.S. Worz, J.M. Antonietti, S. Abbet, K. Judai, U. Heiz, Charging effects on bonding and catalyzed oxidation of CO on Au8 clusters on MgO, Science 307 (2005) 403–407.
[46] B. Alinejad, K. Mahmoodi, Hydrogen generation from water and aluminum promoted by sodium stannate, Int. J. Hydrog. Energy 34 (2009) 7934–7938.
[47] B. Strohmeier, An ESCA method for determining the oxide thickness on aluminum alloys, Surf. Interface Anal. 15 (1990) 51–56.
[48] N.A. Thorne, P. Thuery, A. Frichet, P. Gimenez, A. Sartre, Hydration of oxide films on aluminium and its relation to polymer adhesion, Surf. Interface Anal. 18 (1990) 236240.
[49] M. Amstutz, M. Textor, Applications of surface-analytical techniques to aluminium surfaces in commercial semifabricated and finished products, Surf. Interface Anal. 19 (1992) 595–600.
[50] D.T.Y. Chen, DSC dehydration peaks and solubility products of $Al(OH)_3$, Thermochim. Acta 11 (1975) 101–104.
[51] J.M.R. Mercury, P. Pena, A.H. De Aza, D. Sheptyakov, X. Turrillas, On the decomposition of synthetic gibbsite studied by neutron thermodiffractometry, J. Am. Ceram. Soc. 89 (2006) 3728–3733.
[52] A.D.V. Souza, C.C. Arruda, L. Fernandes, M.L.P. Antunes, P.K.K. Kiyohara, R. Salomao, Characterization of aluminum hydroxide ($Al(OH)_3$) for use as a porogenic agent in castable ceramics, J. Eur. Ceram. Soc. 35 (2015) 803–812.
[53] B.K. Gan, I.C. Madsen, J.G. Hockridge, In situ X-ray diffraction of the transformation of gibbsite to alfa-alumina through calcination: effect of particle size and heating rate, J. Appl. Crystallogr. 42 (2009) 697–705.
[54] H. Wang, B. Xu, P. Smith, M. Davies, L. De Silva, C. Wingate, Kinetic modelling of gibbsite dehydration/amorphization in the temperature range 823–923 K, J. Phys. Chem. Solids 67 (2006) 2567–2582.
[55] B. Whittington, D. Ilievski, Determination of the gibbsite dehydration reaction pathway at conditions relevant to Bayer refineries, Chem. Eng. J. 98 (2004) 89.
[56] J. Rouquerol, F. Rouquerol, M. Granteaume, Thermal decomposition of gibbsite under low pressures: I. Formation of the boehmitic phase, J. Catal. 36 (1975) 99–110.
[57] A.M. Trunov, M. Schoenitz, X. Zhu, E.L. Dreizin, Effect of polymorphic phase transformations in Al_2O_3 film on oxidation kinetics of aluminum powder, Combust. Flame 140 (2005) 310–318.
[58] M. Saravanan, R.M. Pillai, B.C. Pai, M. Brahmakumar, K.R. Ravi, Equal channel angular pressing of pure aluminium—an analysis, Bull. Mater. Sci. 29 (2006) 679–684.
[59] R. Casati, F. Bonollo, D. Dellasega, A. Fabrizi, G. Timelli, A. Tuissi, M. Vedani, Ex situ Al–Al_2O_3 ultrafine grained nanocomposites produced via powder metallurgy, J. Alloy. Compd. 615 (2014) S386–S388.
[60] R.J. Arsenault, N. Shi, Dislocation generation due to differences between the coefficients of thermal-expansion, Mater. Sci. Eng.: A 81 (1986) 175–187.